


Experimental investigation of the abnormal rise of water-wings downstream of a step-type aerator

Hu Han ^{a,*}, Huang Guobing^a, Wang Zhixin^a and Huang Lu^b

^a Changjiang River Scientific Research Institute, Wuhan 430010, China

^b Lancang-Mekong Water Resources Cooperation Center, Beijing 100000, China

*Corresponding author. E-mail: huhan@mail.crsri.cn

 HH, 0000-0001-8780-0235

ABSTRACT

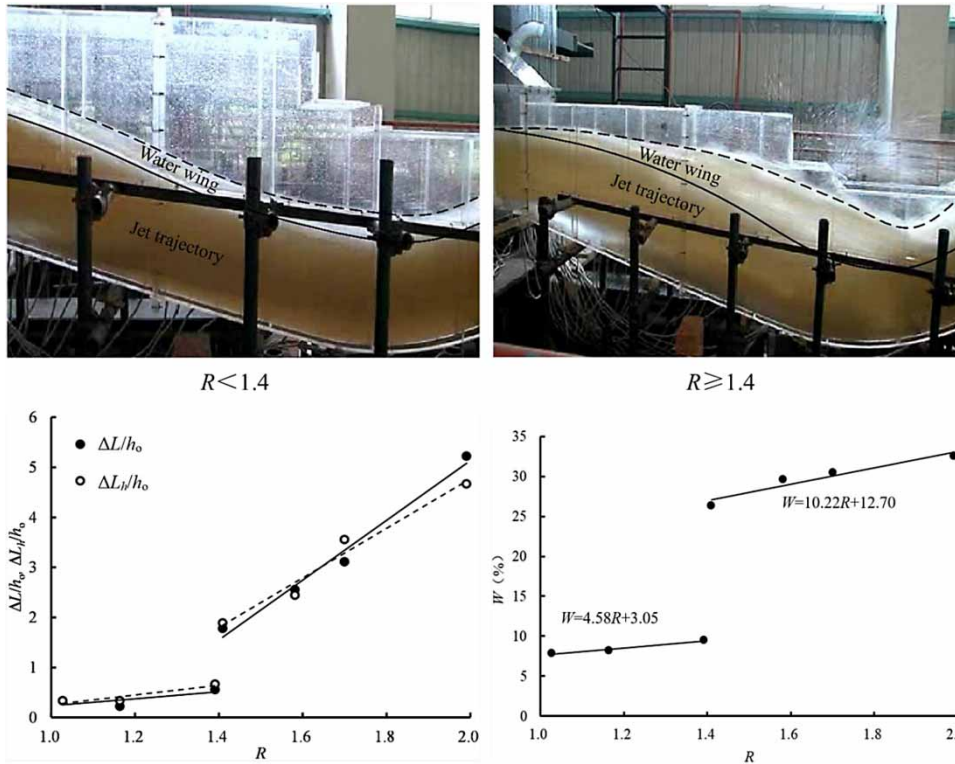
In the prototype observation of a huge water conservancy project, flood discharge in the deep outlets showed strong fluctuations in the downstream of step-type aerators. Intermittent eruption and rise of the water-wing was observed, and the water-wing occasionally impacted on the structures above the chute. In order to investigate the mechanism of water-wing rise, model tests of the deep outlet have been conducted. High-speed camera, pressure sensors, and hot-wire anemometer are adopted to obtain the characteristics of cavity and water-wing. Several key parameters are measured, including air pressure in the cavity and air entrainment volume. It is found that variations of net cavity length, filling water length, and the height of water-wing rise increase with the angle ratio R , and a substantial jump occurs for all related parameters when R approaches 1.4. The rate of water-wing rise W is less than 10% for $R < 1.4$, while it suddenly increases to over 25% for $R > 1.4$. Correlations among inflow condition, jet impact angle, cavity deformation, pressure fluctuation in the cavity, and the rise of water-wing are studied, thus the underlying mechanism of abnormal rise of water-wing is proposed.

Key words: aerators, air entrainment, cavity characteristics, model test, water-wing

HIGHLIGHTS

- Abnormal rise of water-wing downstream of a step-type aerator is studied by the model test.
- The correlation among incoming flow conditions, aeration cavity length, filling water length, air entrainment volume, and water-wing rising has been studied.
- The mechanism of abnormal rise of the water-wing is revealed.

GRAPHICAL ABSTRACT



1. INTRODUCTION

With the vigorous development of the hydropower industry in the last 20 years, many high dams or ultra-high dams have been constructed. In terms of flood discharge and energy dissipation, the majority of these large hydropower projects are characterised with high water head, large flow rate, high discharge power, and complex geological conditions. Generally, the maximum velocity of flood discharge flow can reach up to 50 m/s, and this leads to a few destructive issues, for example cavitation erosion on the chute surface (Wu *et al.* 2013), difficulties in energy dissipation and scour prevention (Zhang & Niu 2014), eruption and rise of a water-wing (Han *et al.* 2006), atomisation of flood discharge (Huang *et al.* 2017a, 2017b), and vibration of hydraulic structures (Ma *et al.* 2020). These issues have become significant to the design and operation safety of hydropower projects. Turbulent motions of high-speed flood discharge flow are usually manifested as cavitation, aeration, water-wing eruption, and strong pressure fluctuations (Huang *et al.* 2017a, 2017b). In particular, eruption and rise of a water-wing, caused by step-type aerators under high water head conditions, could potentially lead to safety issues of certain structures (Toyoshima *et al.* 2003; Hunt & Kadavy 2015).

In the prototype observation of a huge water conservancy project (Huang *et al.* 2017a, 2017b), it was observed that, during the flood discharge under high water head conditions, flow in the open-channel section of the deep outlets showed abnormally strong fluctuations after passing through the step-type aerator. The surface of the flow went up and down intermittently, with the water-wing impacting on the cover plate of the chute. In addition, noticeable vibration was observed for buildings on the dam. The eruption and rise of the water-wing caused considerable concerns to the safety of the project. A typical cycle of the eruption and rise of a water-wing is shown in Figure 1.

A water-wing is a common hydraulic phenomenon during flood discharge of discharge structures with sudden change of cross section. A water-wing not only causes safety issues of hydraulic structures, but leads to secondary environmental damages such as scour of downstream slopes and flood discharge atomisation. The water-wing phenomenon has been studied extensively in the past to reveal its formation mechanism, potential damages, and influence on hydraulic structures, among others Han *et al.* (2006) studied different hydraulic characteristics of water-wings on stepped spillways of various sizes. Huang

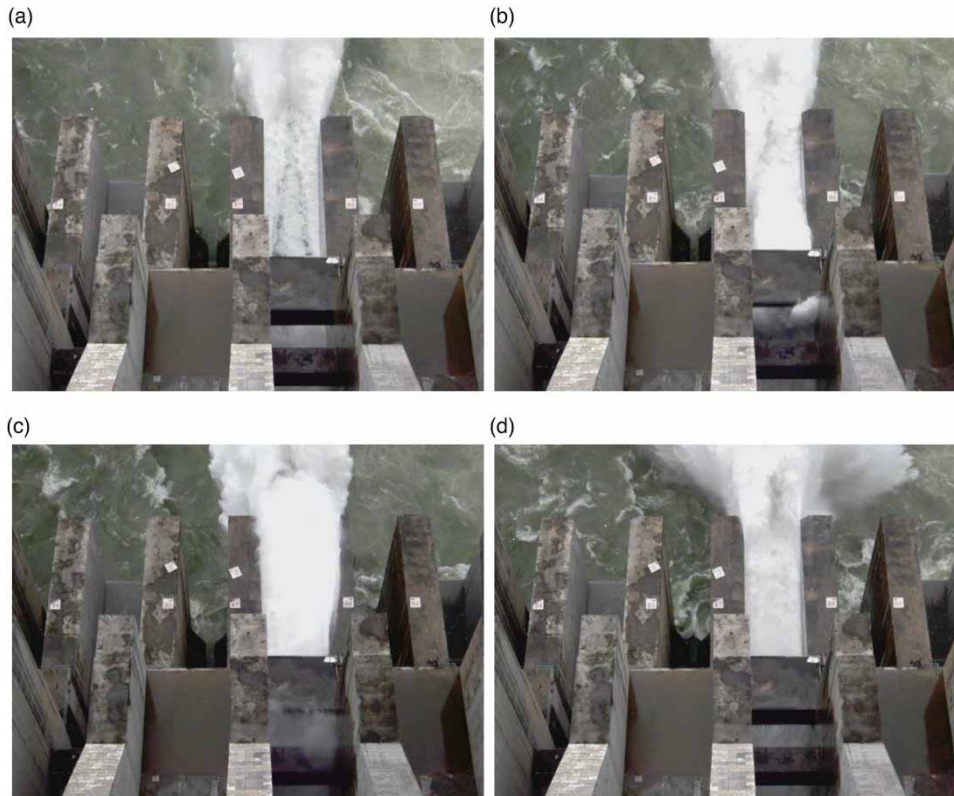


Figure 1 | A cycle of water-wing rise in the deep outlet of a large water conservancy project. (a) Discharging flow in normal condition. (b) Initial stage of the water-wing eruption. (c) Rise of the water-wing reached the maximum height and impacted on the cover plate of the chute. (d) The water-wing went down and discharging flow returned to normal condition.

et al. (2017a, 2017b) revealed the formation mechanism of shock waves and water-wings of slit-type energy dissipators, and proposed a novel method for estimating the coverage area of water-wings.

Unlike aeration of flows down stepped chutes (Chanson & Toombes 2002; Felder & Chanson 2013; Zhang & Chanson 2018; Nina *et al.* 2022) and aeration of hydraulic jumps (Felder & Chanson 2018; Tang *et al.* 2021), air is mostly entrained into the high-speed flows over aerators through the lower interface in the cavity, and through the upper free surface in the atmosphere. It is known that cavity characteristics are critical to the effect of aerators, thus the prevention of cavitation damage. The process of air entrainment could be divided into four parts, and it is of great relevance to the jet trajectory (Chanson 1989). In worst cases, an aerator can be fully filled with water, and act as a cavitation generator itself (Chanson 1995). Air-water flow properties and structures of high-speed flows downstream spillway aerators, however, are rather challenging to obtain by means of prototype observation. Yang *et al.* (2000) established a predictive model to calculate hydraulic and aeration characteristics, and proposed formulae to estimate cavity length, negative pressure in the cavity, and air entrainment volume under low Froude number conditions. Ma & Wu (2012) proposed two threshold values for flow regime conversions (Wu & Ma 2013) below an aerator, and Wu *et al.* (2011) suggested that the filling water in the cavity affects directly the air entrainment behaviour. Furthermore, Wu *et al.* (2013) and Wang *et al.* (2019) studied characteristics of the bottom roller inside the cavity below an aerator, and the filling water is found to be controllable for certain impact angles (Qian *et al.* 2014). Bai *et al.* (2018a) divided the chute downstream of the aerator into four characteristic zones, and found that only part of the air entrained in the cavity was entrained into the flow. A close relationship between the air bubble frequency and air concentration was also observed for open-channel flows downstream of the aerators (Bai *et al.* 2018b). Regarding entrained air characteristics at spillway aerators, a few numerical studies using turbulence modelling demonstrated reasonable agreement with experimental measurements and prototype observations (Shilpakar *et al.* 2017; Yang *et al.* 2019; Aydin *et al.* 2020; Sarwar *et al.* 2020), yet typical RANS (Reynolds-averaged Navier-Stokes) simulations may be somewhat inadequate in investigating instantaneous flow motions similar to that observed in the present study.

To the authors' best knowledge, the intermittent eruption and rise of a water-wing behind step-type aerators, as observed in the present study, has not been reported in other hydraulic projects. Besides, previous studies on spillway aerators mainly focus on cavity characteristics, and not much attention was paid to the behaviour of the upper free surface. The abnormal motions of the water-wing are yet to be well investigated, let alone understood.

According to the typical shape of the cavity below an aerator, four parameters are defined in this study, the jet length L_s , the net cavity length L , the length of filling water L_h , and the impact angle of the jet α , as shown in Figure 2. The Froude number of the incoming flow Fr is defined as

$$Fr = \frac{v}{\sqrt{gh_0}} \quad (1)$$

where, h_0 and v are, respectively, the depth and average velocity at the exit of the pressure section of the deep outlet, and g is the gravitational acceleration.

The amplitude of net cavity length variation ΔL is defined as the difference between the maximum and minimum values of L . Similarly, the amplitude of filling water length variation ΔL_h is defined as the difference between the maximum and minimum values of L_h . In this paper, h_0 is chosen as the characteristic length for nondimensionalisation of L_s , L , ΔL , L_h , ΔL_h .

In order to quantify the intensity of the rise of the water-wing, the rate of rise W is defined as the ratio of the maximum rise to the water depth at the same position:

$$W = \frac{h_w}{h} \quad (2)$$

In order to investigate the abnormal eruption and rise of the water-wing downstream of the step-type aerator, a series of model tests were carried out in the present study. Variations of jet trajectories, cavity characteristics, and air concentration were measured, and their relationships with upstream water head analysed. Conditions of emergence and excitation mechanism of the rise are also discussed.

2. METHODS

2.1. Experimental setup

In model tests, scale effect usually has some influence on the hydraulic characteristics compared with prototype data such as air entrainment (Lian *et al.* 2017). The smaller the model scale, the larger the difference between model and prototype. The focuses of this study are cavity characteristics below a spillway aerator and unsteady motions of the water-wing. Therefore, selection of the model scale is of great importance, considering the scale effect on aerated high speed flows. Chen (1992) and Xia & Zhang (1996) compared the air entrainment concentration between model test and prototype observation for Fengjia-shan spillway and Foz do Areia spillway, with the model scale range from 1/8 to 1/50. Their results showed that scale effect is negligible only when flow velocity reaches more than 6 m/s in the model test, such that air concentration obtained can be converted to that of the prototype by Froude scaling.

In the present experimental work, a physical model of the deep outlet of a huge water conservancy project is designed according to gravity similarity, and the model scale is 1/25. A flow velocity larger than 6 m/s is achieved in our experiments.

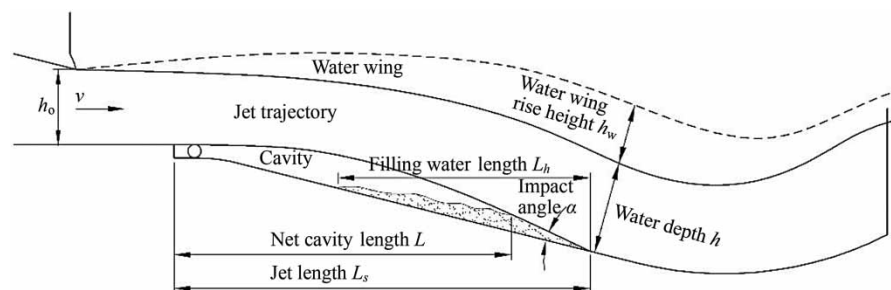


Figure 2 | Schematic of the cavity below a step-type aerator.

Flow properties and air entrainment characteristics should not be greatly affected by the chosen model scale, according to previous studies. Thus, the current physical model is considered appropriate for our study.

The deep outlet consists of a short pressure tube with a horizontal length of 18.7 m, a vertical drop of 1.5 m in height, a horizontal section of 2.85 m, a slope with a ratio of 1/4 (the horizontal projection length is 44.5 m), followed by a flip bucket with a radius of 40 m at the end. The air intake orifice is set on the sidewall of the 2.85 m horizontal section, and located at 2.15 m behind the step (see Figure 3). The diameter of the air intake well is 1.4 m. In summary, the deep outlet adopts a short pressure tube with vertical drop aeration, followed by an open-flow chute with a flip bucket.

The test apparatus is composed of an upstream tank that can provide a 4.0 m water head (equivalent to 100.0 m water head of the prototype), a step-type aerator, and a downstream pool. To facilitate observation and measurements, the whole deep outlet model is made of plexiglass.

2.2. Instrumentation

Observation of air–water flow patterns was facilitated with a Revealer™ high-speed camera (Model 5F02M). The flow rate Q was measured with a Krohne™ electromagnetic flowmeter (OPTIFLUX 6000) installed before the upstream tank. The range of measurement is 0–200 L/s, and the accuracy is 0.2 L/s. The wind speed or ventilation capacity of the air intake orifice was measured by a hot-wire anemometer (Testo 425). The range of measurement is 0–20 m/s, and the accuracy is 0.01 m/s. The fluctuating pressure on the bottom and the sidewall downstream of the step-type aerator was measured by HM90 high-frequency fluctuating pressure sensors. These sensors were excited by an electronic system with a sampling frequency of 1 kHz. The range of measurement of these sensors is 0–100 kPa, with an accuracy of 0.1% FS (full scale).

2.3. Experimental conditions and methodology

According to the actual operating conditions of the prototype project, the upstream water head ranges from 45.0 m to 90.4 m (the corresponding Fr is in the range of 2.49–3.74). Seven typical test conditions are selected to conduct the experiments (see Table 1). For all test conditions, the gate is fully opened.

In this experimental work, the measurement of a parameter (L , L_s , L_h , α , etc.) under a certain test condition was repeated at least four times, and its value presented in this paper refers to the time-averaged value. Considering the influence of the unsteady cavity motions, the chosen sampling duration and frequency were sufficient to obtain reasonable time-averaged flow data, and this was confirmed by increasing the sampling duration and frequency.

3. RESULTS AND DISCUSSION

3.1. Overall flow patterns

It is observed in the experiments that a full cavity is formed below the step-type aerator under all test conditions, after the flow comes out of the short pressure tube. A certain amount of filling water in the cavity is observed for all the cases. Aeration of flow happens at both the lower and upper surfaces of the jet downstream of the aerator, and air bubbles entrained move with the flow towards the outlet of the chute. A water-wing occurs on the upper surface of the jet, and its height changes along the

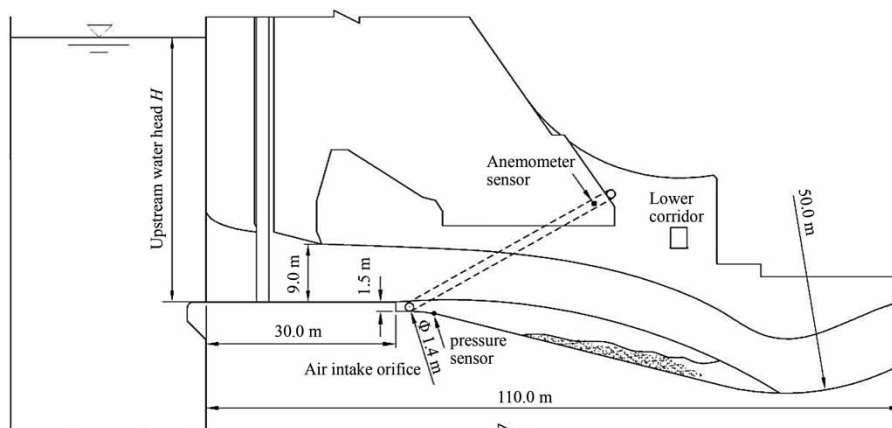


Figure 3 | Schematic of the deep outlet of a huge water conservancy project.

Table 1 | Test conditions

Conditions	C1	C2	C3	C4	C5	C6	C7
H (m)	45.0	55.0	65.0	77.0	82.6	85.0	90.4
Q (m ³ /s)	1,475	1,673	1,848	2,032	2,097	2,125	2,216
Fr	2.49	2.83	3.12	3.43	3.54	3.59	3.74

chute. Under some flow conditions, the jet impacts on the bottom surface of the chute within the flip bucket section, accompanied by splashing and collision of water droplets. High intensity turbulence is observed near the flip bucket.

Figure 4 shows the typical air–water flow patterns downstream of the aerator for both high and low Fr conditions. When the inflow Fr is low (less than 3.43), the water-wing is observed only just above the upper surface of the discharge flow. Turbulence intensity of the flow is weak, and the flow patterns upstream and downstream of the aerator are relatively stable. No obvious rise of the water-wing is seen under this condition. However, when the inflow Fr is high enough (reaching 3.43), turbulence to a certain extent is observed for the flow between the exit of the short pressure section and the step-type aerator. Then, turbulence intensity of the flow is aggravated by the aerator. Downstream of the aerator, intermittent eruption and rise of a water-wing occur, and it occasionally splashes on the structures above. The frequency and strength of splash increase with the inflow Fr . When the inflow Fr reaches 3.54, the water-wing sometimes even hits the lower corridor above the chute.

The above observations show that turbulence of flow in the deep outlet becomes more intense with higher inflow Fr . As a result, the water-wing rises, hitting the structures above. The jet also exhibits strong oscillations downstream of the aerator. These flow patterns observed in the model test are consistent with those of the prototype.

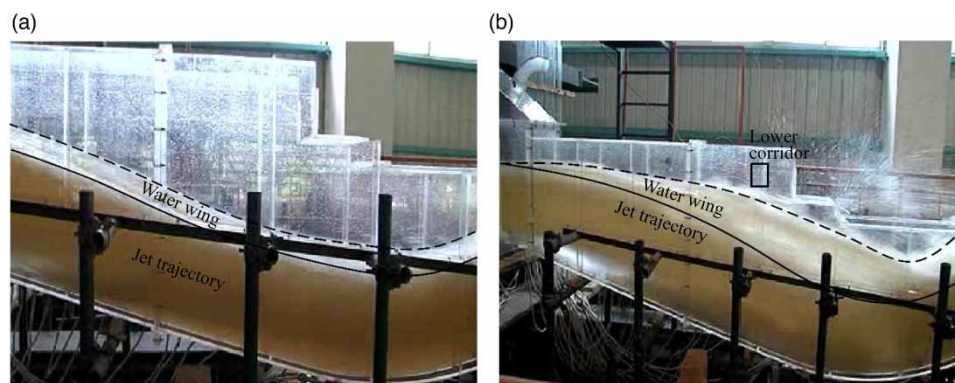
3.2. Cavity characteristics

Cavity characteristics consist of jet length, jet trajectory, length of filling water, and net cavity length. The relationship between jet length L_s and inflow Fr is shown in Figure 5. The model test results are in good agreement with the theoretical calculations proposed by Chanson (1995). It can be seen from the figure that the jet length increases almost linearly with increasing Fr of the inflow.

Besides the variation jet length, the impact angle of the jet α also varies with the inflow condition. Jet trajectory and the impact angle α under each test condition are shown in Figure 6.

It is clear that, with the increase of the inflow Fr , the impact angle α first decreases and then increases. With regard to flow patterns, the larger the impact angle is, the more unstable the flow becomes. Meanwhile, the amount of filling water increases, leading to a significant variation in the net cavity length. Under conditions C1–C3 ($\alpha < 15.5^\circ$), variation in the length of filling water is not obvious, and the cavity is relatively stable, whereas under conditions C4–C7 ($15.5^\circ \leq \alpha < 22^\circ$), the length of filling water fluctuates strongly, and the volume of the cavity changes dramatically.

Wang *et al.* (2009) carried out numerical simulations to capture detailed flow structures behind a step-type aerator. They concluded that the filling water in the cavity is mainly affected by the impact angle α , and the distribution range of the jet in

**Figure 4** | Typical flow patterns in the open-channel section of the deep outlet. (a) $Fr < 3.43$; (b) $Fr > 3.43$.

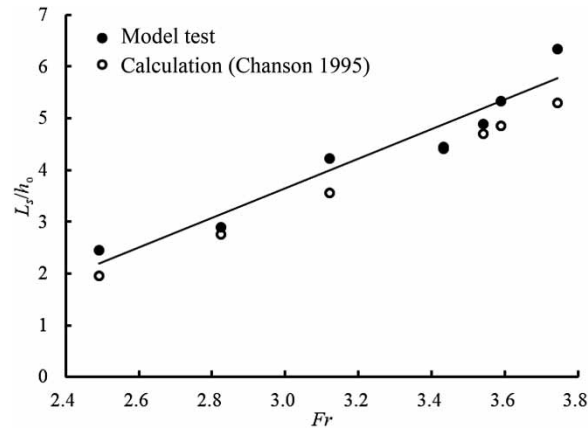


Figure 5 | Relationship between the jet length and inflow Fr .

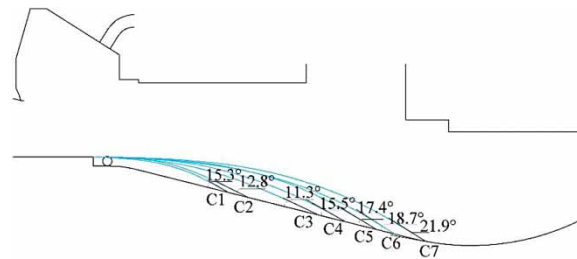


Figure 6 | Impact angle α under each test condition.

the impact zone. When the impact angle is small, and the distribution ranges of the jet are close in the longitudinal and transverse directions, filling water is hardly seen in the cavity. Xu *et al.* (2009) studied the aerated flow behind a step-type aerator using the jet trajectory equation and the cavity filling water equation. They suggest that for a fixed bottom slope, the larger the impact angle, the easier for the cavity to be filled. When the impact angle is small enough, no filling water exists in the cavity.

The relationship between the length of filling water and the impact angle is shown in Figure 7. The length of filling water shows a linear increase with the increasing impact angle, and the relationship between them could be expressed by means of regression analysis as

$$L_h/h_0 = 0.26\alpha - 2.86 \quad (3)$$

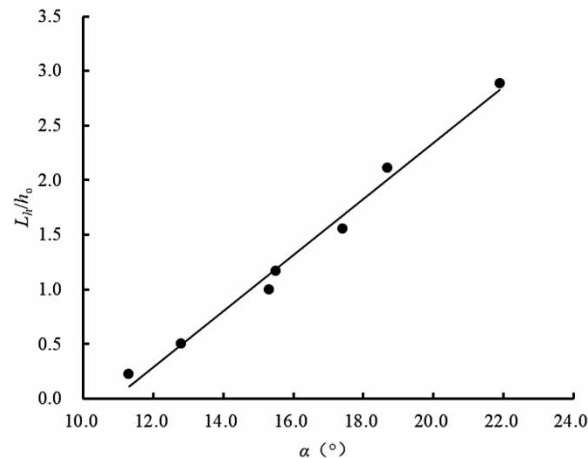


Figure 7 | Relationship between the length of filling water L_h/h_0 and the impact angle α .

According to the equation, when the impact angle α is 11.0° , no filling water is present in the cavity. In this study, we define $\alpha = 11.0^\circ$ as the critical impact angle. Based on this, when α is larger than the critical value, filling water occurs in the cavity, and eventually the oscillation of filling water leads to the change of net cavity length (or volume of cavity).

In order to compare the effect of impact angle on cavity characteristics, a dimensionless parameter R is introduced, and it is defined as the ratio of the impact angle α to the critical impact angle (11.0°). It is noted from Figure 6 that, when the inflow Fr is larger than 3.43, the angle ratio R increases with Fr . This is also when abnormal rise of the water-wing happens. Variations of nondimensionalised ΔL and ΔL_h with the angle ratio R are shown in Figure 8.

It can be seen that, under conditions C1–C3, where the angle ratio R is low ($R < 1.4$), only slight variations are shown for the net cavity length and the length of filling water. This means that the cavity is relatively stable. However, under conditions C4–C7, where $R > 1.4$, an obvious jump appears in both ΔL and ΔL_h . Furthermore, ΔL and ΔL_h increase linearly with R .

3.3. Air entrainment

The average volume of air entrained into the air intake well is shown in Figure 9, together with the inflow Fr under each test condition. The prototype data (Duan *et al.* 2019) obtained from the same water conservancy project are also included for comparison. Note that, in order to compare with the prototype data, the values of the model test have been converted according to the principle of similarity.

It is shown clearly that the volume of air entrainment obtained in the model test is in good agreement with the prototype observation. This further proves that the present model scale is suitable. It is also observed that, similar to the jet length, the average volume of air entrainment Q_{air} increases linearly with the inflow Fr .

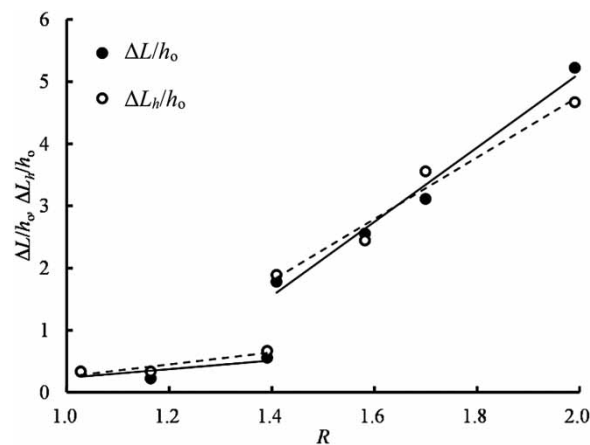


Figure 8 | Variations of $\Delta L/h_0$ and $\Delta L_h/h_0$ with the angle ratio R .

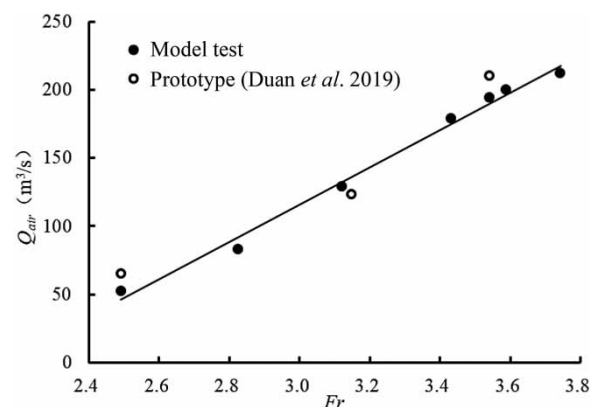


Figure 9 | Relationship between average air entrainment volume Q_{air} and the inflow Fr .

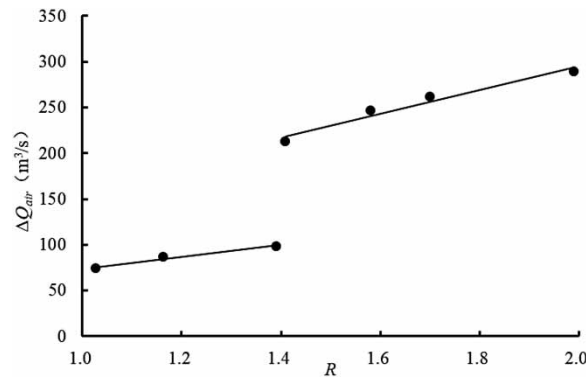


Figure 10 | Relationship between the variation of air entrainment volume ΔQ_{air} and the angle ratio R .

Fluctuation of the air entrainment volume also represents the stability of the cavity. The relationship between the variation of air entrainment volume ΔQ_{air} (defined as the difference between the maximum and minimum values of volume of air entrainment) and the angle ratio R is shown in Figure 10.

Overall, ΔQ_{air} increases with the angle ratio R (or the impact angle). It is worth noticing that a sudden jump again appears when R approaches 1.4. The behaviour of ΔQ_{air} is similar to that of ΔL and ΔL_h as shown previously in section 3.2. This result indicates a certain correlation between the cavity instability and air entrainment fluctuation.

3.4. Rise of the water-wing

A water-wing was formed downstream of the short pressure tube under all the test conditions. The height of water-wing rise, however, differs between test conditions, in particular when the angle ratio R reaches 1.4. Trajectories of the water-wing rise under typical conditions were observed, and the outlines of water-wing rise under typical conditions are shown in Figure 11. It can be seen that the rise of the water-wing becomes distinctively large from condition 4. When the inflow Fr is high, turbulence of the flow is intensified, and the water-wing occasionally rises and impacts on the structures above.

As observed in the experiments, the intermittent eruption and rise of the water-wing is often accompanied by strong turbulence of the flow, dramatic changes in the cavity shape, and a large variation of air entrainment volume. Variation of the rate of water-wing rise with the angle ratio R is shown in Figure 12. Overall, the rate of water-wing rise W increases with the angle ratio R . Yet again, an evident jump in W appears when R approaches 1.4. Under conditions C1–C3, where the angle ratio is smaller than 1.4, no obvious rise of the water-wing is observed, and the rate of water-wing rise W is less than 10%. While Under conditions C4–C7, where the angle ratio R is greater than 1.4, the height of the water-wing suddenly rises to more than 25% of the water depth, and then increases linearly with the angle ratio R . When the impact angle α is twice the critical impact angle, i.e. $R = 2$, the amplitude of water-wing rise reaches 33% of the water depth. The relationship between W and R could be expressed by means of regression analysis as follows.

$$\begin{cases} W = 4.58R + 3.05 & R < 1.4 \\ W = 10.22R + 12.70 & R \geq 1.4 \end{cases} \quad (4)$$

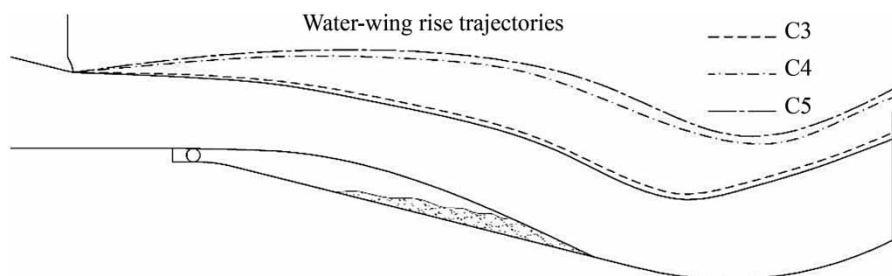


Figure 11 | Outlines of water-wing rise under typical conditions.

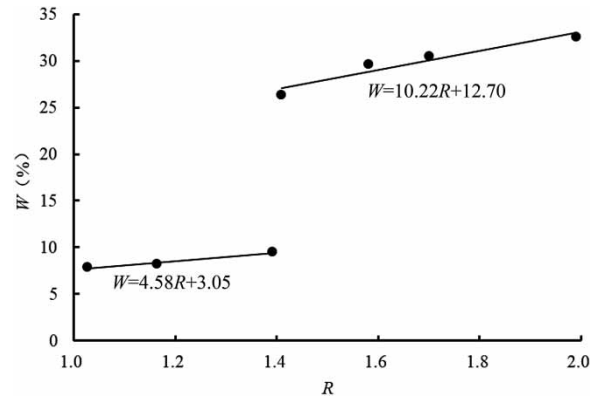


Figure 12 | Relationship between the rate of water-wing rise W and the angle ratio R .

The behaviour of water-wing rise is very similar to that of ΔQ_{air} as shown in Figure 10. It seems that a higher rate of water-wing rise is associated with a larger variation of air entrainment volume.

3.5. Mechanism of water-wing rise

Similar relationships with the angle ratio R are shown for variations of net cavity length $\Delta L/h_o$ and filling water length $\Delta L_h/h_o$, variation of air entrainment volume ΔQ_{air} , and the rate of water-wing rise W , as in Figures 8, 10 and 12. Under conditions C1–C3, where the angle ratio R is small ($R < 1.4$), $\Delta L/h_o$, $\Delta L_h/h_o$, ΔQ_{air} , and W increase moderately with R . As soon as the angle ratio reaches 1.4, a dramatic jump occurs. Then these parameters keep increasing with R at a higher rate. The experimental results suggest intrinsic correlations of these four parameters.

To further investigate the underlying mechanism of abnormal rise of the water-wing, temporal variations of pressure fluctuation in the cavity and height of water-wing rise were monitored in the experiments. Time histories of the variations are shown in Figure 13. A short phase difference of approximate 2 seconds is noted from the figure, and sharp pressure increase in the cavity occurs ahead of the substantial rise of the water-wing. It can be seen that the dramatic rise of the water-wing is highly correlated with pressure fluctuation in the cavity.

Based on the above analysis, a mechanism is proposed for the abnormal rise of the water-wing downstream of a step-type aerator. That is, the impact angle of the jet is determined by the inflow condition, i.e., Fr . When the impact angle becomes larger than a critical value, variations of net cavity length and filling water length, which show a sudden increase, cause

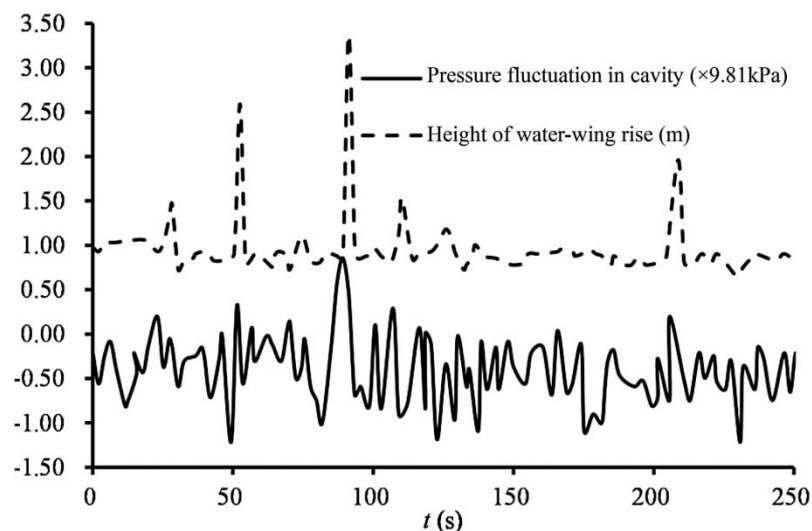


Figure 13 | Time histories of pressure fluctuation in the cavity and height of water-wing rise.

pressure fluctuations in the cavity. As a result, a dramatic rise of the water-wing emerges. The whole process keeps going, and the abnormal rise of the water-wing is observed from time to time.

4. CONCLUSIONS

- (1) During flood discharge in the deep outlets of a huge water conservancy project, abnormal eruption and rise of a water-wing were observed downstream of the step-type aerators. Model tests have been conducted to reproduce and investigate this phenomenon. The rate of water-wing rise W is found to increase with the Froude number Fr of the inflow upstream of the aerator. Under the condition of $Fr < 3.43$, W is less than 10%. However, a dramatic jump occurs when Fr reaches 3.43 or higher, and W increases up to 25–33%.
- (2) Variations of net cavity length $\Delta L/h_o$ and length of filling water $\Delta L_h/h_o$, variation of air entrainment volume ΔQ_{air} , and the rate of water-wing rise W all have a similar relationship with the angle ratio R . When the angle ratio R is small ($R < 1.4$), these parameters increase moderately with R . A substantial jump occurs when R approaches 1.4, and then these parameters keep increasing with R at a higher rate.
- (3) The abnormal rise of the water-wing downstream of step-type aerators is related to the impact angle of the jet. The underlying mechanism of the emergence of this phenomenon could be summarised as follows. The impact angle of the jet varies with the inflow condition (Fr). As a result, the shape of the cavity deforms. Then the pressure in the cavity changes accordingly. It is shown that sharp pressure increases in the cavity are responsible for the dramatic rise of the water-wing.

FUNDING

This work was supported by National Natural Science Foundation of China (Grant No. 51879013), and Central Public-Interest Scientific Institution Basal Research Fund (Grant No. CKSF2019394/GC).

CONFLICTS OF INTEREST

The authors declare no conflict of interest. The funders had no role in the design of the study; in the collection, analyses, or interpretation of data; in the writing of the manuscript, or in the decision to publish the results.

DATA AVAILABILITY STATEMENT

All relevant data are included in the paper or its Supplementary Information.

REFERENCES

- Aydin, M. C., Isik, E. & Ulu, A. E. 2020 Numerical modeling of spillway aerators in high-head dams. *Applied Water Science* **10** (1), 1–9.
- Bai, R., Liu, C., Feng, B., Liu, S. & Zhang, F. 2018a Development of bubble characteristics on chute spillway bottom. *Water* **10** (9), 1129.
- Bai, R., Liu, S., Tian, Z., Wang, W. & Zhang, F. 2018b Experimental investigation of air-water flow properties of offset aerators. *Journal of Hydraulic Engineering* **144** (2), 04017059.
- Chanson, H. 1989 Study of air entrainment and aeration devices. *Journal of Hydraulic Research* **27** (3), 301–319.
- Chanson, H. 1995 Predicting the filling of ventilated cavities behind spillway aerators. *Journal of Hydraulic Research* **33** (3), 361–372.
- Chanson, H. & Toombes, L. 2002 Air–water flows down stepped chutes: turbulence and flow structure observations. *International Journal of Multiphase Flow* **28** (11), 1737–1761.
- Chen, C. 1992 Experimental studies on scale modelling in vacuum tank and mitigating cavitation damage by aeration. In *Proceedings of International Symposium on Hydraulic Research in Nature and Laboratory*, Vol. I, Wuhan.
- Duan, W. G., Hou, D. M., Wang, C. H., Hu, H. & Tang, X. F. 2019 Hydraulic prototype observation and analysis of Three Gorges Dam discharge structures. *Journal of Hydraulic Engineering* **50** (11), 1339–1349.
- Felder, S. & Chanson, H. 2013 Aeration, flow instabilities, and residual energy on pooled stepped spillways of embankment dams. *Journal of Irrigation and Drainage Engineering* **139** (10), 880–887.
- Felder, S. & Chanson, H. 2018 Air–water flow patterns of hydraulic jumps on uniform beds macroroughness. *Journal of Hydraulic Engineering* **144** (3), 04017068.
- Han, Y., Feng, R. L., Tian, J. N. & Li, B. L. 2006 Water-wing on steep slope of stepped spillways. *Journal of Hydroelectric Engineering* **25** (01), 114–118.
- Huang, G. B., Du, L., Wang, C. H. & Nie, Y. H. 2017a Water-wing trajectory and characteristics of rainfall in slit-type bucket. *Journal of Yangtze River Scientific Research Institute* **34** (12), 44–47.

- Huang, G. B., Hu, H., Wang, C. H. & Du, L. 2017b Shock waves and water wing in slit-type energy dissipaters. *Journal of Hydrodynamics* **29** (03), 504–509.
- Hunt, S. L. & Kadavy, K. C. 2015 Discussion of ‘Aeration, flow instabilities, and residual energy on pooled stepped spillways of embankment dams’ by Stefan Felder and Hubert Chanson. *Journal of Irrigation and Drainage Engineering* **141** (2), 07014038.
- Lian, J. J., Qi, C. F., Liu, F., Guo, W. J., Pan, S. Q. & Ouyang, Q. 2017 Air entrainment and air demand in the spillway tunnel at the Jingping-I Dam. *Applied Sciences* **7** (9), 930.
- Ma, B., Ge, J. Z., Liang, S. & Lian, J. J. 2020 Study on characteristics of vibration in the foundation and ground induced by flood discharge and optimization of flood discharge scheme of high arch dam. *Journal of Tianjin University (Science and Technology)* **53** (01), 27–34.
- Ma, F. & Wu, J. H. 2012 Flow regimes below aerators for discharge tunnels. *Journal of Hydrodynamics* **24** (3), 378–382.
- Nina, Y. A., Shi, R., Wüthrich, D. & Chanson, H. 2022 Intrusive and non-intrusive two-phase air-water measurements on stepped spillways: a physical study. *Experimental Thermal and Fluid Science* **131**, 110545.
- Qian, S. T., Wu, J. H., Ma, F., Xu, J. R., Peng, Y. & Wang, Z. 2014 Cavity filling water control below aerator devices. *Journal of Hydrodynamics* **26** (3), 424–430.
- Sarwar, M. K., Ahmad, I., Chaudary, Z. A. & Mughal, H. U. R. 2020 Experimental and numerical studies on orifice spillway aerator of Bunji Dam. *Journal of the Chinese Institute of Engineers* **43** (1), 27–36.
- Shilpakar, R., Hua, Z., Manandhar, B., Shrestha, N., Zafar, M. R., Iqbal, T. & Hussain, Z. 2017 Numerical simulation on tunnel spillway of Jingping-I hydropower project with four aerators. *IOP Conference Series Earth and Environmental Science* **82** (1), 012013.
- Tang, R., Bai, R. & Wang, H. 2021 A comparative study of pre-aeration effects on hydraulic jump air–water flow properties at high Froude numbers. *Environmental Fluid Mechanics* **21** (6), 1333–1355.
- Toyoshima, Y., Amano, K. & Tanaka, Y. 2003 Field observation and evaluation of destratification by aeration circulation in a dam reservoir. *Proceedings of Hydraulic Engineering* **47**, 1243–1248.
- Wang, H. Y., Dai, G. Q., Liu, C. & Yang, Q. 2009 Discussion of aerator bottom cavity backflow of discharge structures. *Chinese Journal of Hydrodynamics* **24** (04), 425–431.
- Wang, Y., Wu, J., Ma, F. & Qian, S. 2019 Pressure distribution of bottom rollers below the aerator device. *Water Science and Technology* **79** (4), 668–675.
- Wu, J. H. & Ma, F. 2013 Cavity flow regime for spillway aerators. *Science China (Technological Sciences)* **56** (04), 818–823.
- Wu, J. H., Ma, F. & Dai, H. C. 2011 Influence of filling water on air concentration. *Journal of Hydrodynamics, Series B* **23** (5), 601–606.
- Wu, J. H., Ma, F. & Xu, W. L. 2013 Bottom roller characteristics in cavity of chute aerators. *Journal of Hydraulic Research* **51** (3), 317–321.
- Xia, Y. & Zhang, L. 1996 Comparison of hydraulic characteristics in prototype and model. *Design of Water Resources & Hydroelectric Engineering* (01), 41–49.
- Xu, Y. M., Yang, H. X., Zhao, W. & Wang, H. J. 2009 Effect of chute bottom slope on back water in cavity of jet flow from chute aerator. *Water Resources and Hydropower Engineering* **40** (12), 47–51.
- Yang, J., Teng, P. & Zhang, H. 2019 Experiments and CFD modeling of high-velocity two-phase flows in a large chute aerator facility. *Engineering Applications of Computational Fluid Mechanics* **13** (1), 48–66.
- Yang, Y. S., Yang, Y. Q. & Shuai, Q. H. 2000 The hydraulic and aeration characteristics of low Froude number flow over a step aerator. *Journal of Hydraulic Engineering* (2), 27–31.
- Zhang, C. R. & Niu, Z. P. 2014 Key technology research on flood discharge and energy dissipation of Xiangjiaba Hydropower Station. *Water Resources and Hydropower Engineering* **45** (11), 1–9.
- Zhang, G. & Chanson, H. 2018 Effects of step and cavity shapes on aeration and energy dissipation performances of stepped chutes. *Journal of Hydraulic Engineering* **144** (9), 04018060.

First received 11 November 2021; accepted in revised form 4 March 2022. Available online 17 March 2022